ACS APPLIED MATERIALS & INTERFACES

www.acsami.org

Research Article

Scalable, Flexible, and UV-Resistant Bacterial Cellulose Composite Film for Daytime Radiative Cooling

Yuan-Cheng Ding,[†] Guo-Wei Tang,[†] Hao-Yu Zhao,[*] Jia-Ming Liu, Tian-Hao Fan, Yu-Can Peng, Pin Jern Ker, and Dong-Sheng Geng

Cite This: *ACS Appl. Mater. Interfaces* 2025, 17, 6857−6866

Read Online

ACCESS | Metrics & More | Article Recommendations | Supporting Information

ABSTRACT: Radiative cooling, a passive cooling technology, functions by reflecting the majority of solar radiation (within the solar spectrum of 0.3−2.5 μm) and emitting thermal radiation (within the atmospheric windows of 8−13 μm and 16−20 μm). Predominantly, synthetic polymers are effectively utilized for radiative cooling while posing potential environmental hazards due to their complex components, toxicity, or nonbiodegradation. Bacterial cellulose, a natural and renewable biopolymer, stands out due to its environmentally friendly, scalability, high purity, and significant infrared emissivity. In this work, we developed a bacterial cellulose-based composite film (BCF) with a cross-linked network structure by a facile agitation spraying method to achieve enhanced and sustainable radiative cooling performance. The BCF exhibited superior optical properties and environmental tolerance, with a notable infrared emissivity of 94.6%. As a result, the thermal emitter demonstrates a substantial subambient cooling capacity (11:00 to 13:00, maximum drop of 7.15 °C, average drop of 4.85 °C; 22:00 to 2:00, maximum drop of 2.7 °C, average drop of 2.32 °C). Additionally, the BCF maintained stable emissivity after 240 h of continuous UV irradiation. Furthermore, BCF can effectively preserve the freshness of fruits under intense solar irradiation. Hence, BCF with high radiative cooling performance presents a broad application prospect in building energy conservation, solar cells efficiency enhancement, and food transportation packaging.

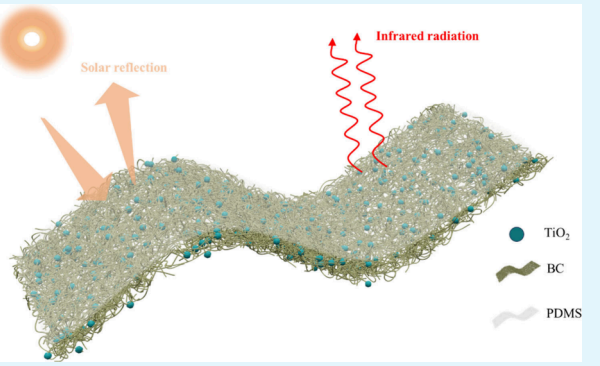

KEYWORDS: *radiative cooling, bacterial cellulose-based composite film, cross-linked network structure, UV resistance, freshness preservation*

INTRODUCTION

The acceleration of global industrialization and population growth has resulted in an increased energy consumption. Attaining carbon neutrality by 2050 stands as a primary global environmental objective to mitigate the energy crisis.[1] Annually, residential buildings account for 40% of global energy consumption, and a substantial portion is consumed by building cooling and air conditioning systems.[2] Consequently, improving the efficiency of existing cooling systems and developing novel refrigeration technologies to bolster building energy efficiency have become imperative.

Radiative cooling (RC) in practice can be realized without external energy input only by leveraging the intrinsic properties and specialized structures of the material naturally. Radiative cooling radiates heat in the form of thermal radiation through the atmospheric window[3−5] (8−13 μm and 16−20 μm) to outer space. At the same time, it scatters or reflects off solar energy within the solar spectrum (0.3−2.5 μm) as much as possible, thereby reducing the heat input and achieving cooling.[6] Effective nighttime radiative cooling relies on a superior infrared radiative performance. However, daytime radiative cooling poses a serious challenge due to direct sunlight and nonradiant heat from the environment. Therefore, the development of novel passive radiative cooling materials with high infrared emissivity and solar reflectivity is of considerable research and application prospects in energy conservation.

Initial research on passive radiative cooling primarily focused on nighttime applications,[7,8] polymers, such as polyethylene (PE),[9,10] polytetrafluoroethylene (PTFE),[3,11] polyamide 6 (PA6),[12,13] and polydimethylsiloxane (PDMS).[14,15] These polymeric materials produce a strong infrared emission effect within the atmosphere transparent window due to the vibrational absorption of the characteristic molecular bonds of C−O−C and C−OH, thereby providing a nighttime radiative cooling effect. As the research progressed, daytime radiative cooling was also proposed. Various structural designs

Received: December 23, 2024
Revised: January 9, 2025
Accepted: January 12, 2025
Published: January 21, 2025

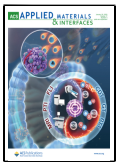

https://doi.org/10.1021/acsami.4c22615
ACS Appl. Mater. Interfaces 2025, 17, 6857−6866

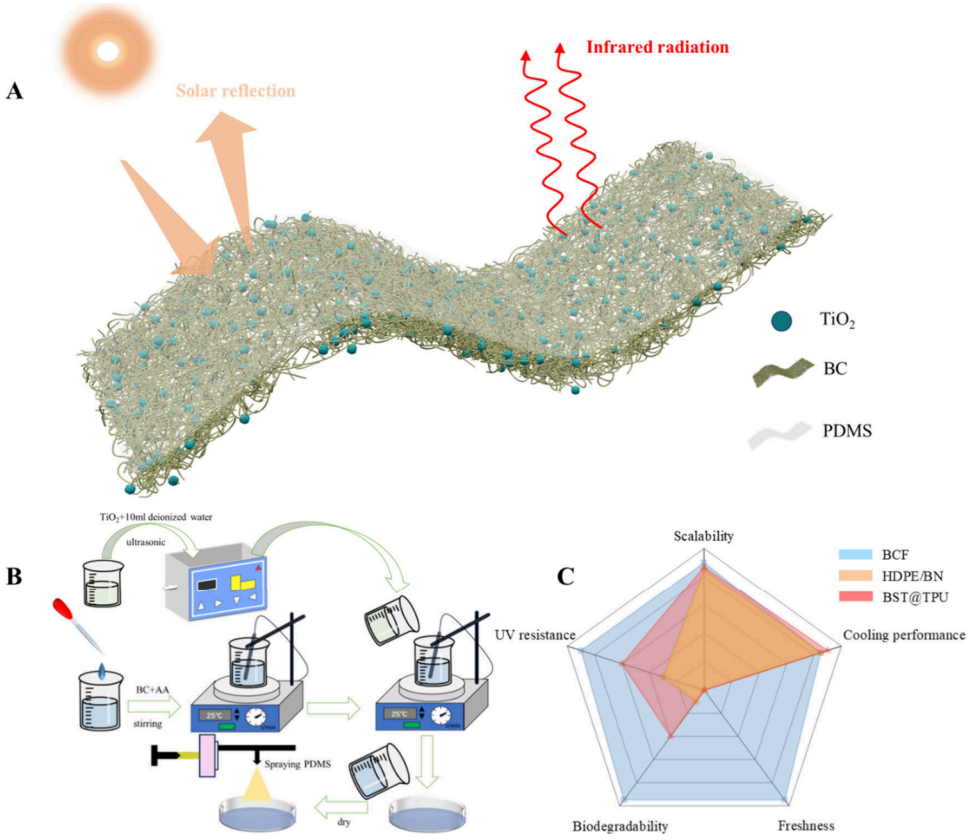

Figure 1. Design strategy and preparation process of bacterial cellulose based radiative cooler: (A) schematic illustration of structural features of BCF; (B) schematic illustration of the fabrication procedure of BCF; (C) advantages of BCF.

have been explored, including particle-doped polymers,[10,16−22] bionics,[23−25] aerogels,[26−28] and porous membranes.[29−31] These materials have been widely applied in building energy efficiency,[9] personal thermal management,[32−37] and photovoltaic cooling.[38] However, some of these technologies, due to their reliance on demanding engineering and manufacturing processes, face difficulties in large-scale production and thus are hard to apply in practical scenarios. In addition, most of these materials are polymer-based, posing issues such as susceptibility to outdoor aging and environmental degradation. Moreover, the production of synthetic polymers, favored for their low cost and processability, entails substantial energy consumption and presents significant ecological impacts, such as refractory microplastics.[39,40]

Cellulose is the most abundant natural macromolecule on earth, representing an inexhaustible and highly valuable renewable resource for human. It is sourced from the terrestrial,[41] plants,[42,43] marine flora,[44] and various bacterium.[45,46] Additionally, cellulose can be derived from seabed organisms and various bacterial metabolites. Due to its natural abundance, biodegradability, and renewability, cellulose has attracted significant interest for radiative cooling applications. Advanced radiative cooling materials have been developed by utilizing diverse cellulose-based substrates. For example, Zhu et al.[47] designed cellulose nanocrystalline films and prepared structurally colored radiatively cooling materials by coating these films onto a highly scattering, porous ethyl cellulose base layer, while the photonic nanostructuring of the substrate led to strong antifading coloration, which consequently resulted in unavoidable solar energy absorption. Cai et al.[48] reported a cellulose composite film composed of cellulose acetate (CA) and TiO_2@potassium titanate (TiO_2@PT) with a solar reflectance of 97% and an emissivity of 95%. Chen et al.[49] prepared cooling lignocellulosic materials by growing inorganic microspheres with phonon-enhanced Fröhlich resonances on fully delignified nanocellulose surfaces. Nonetheless, the purification process of lignocellulose is highly energy-intensive and generates substantial chemical waste. Bacterial cellulose (BC), a biopolymer synthesized by microorganisms, mainly sourced with some specific bacteria such as *Acetobacter* and *Agrobacterium*.[50] Compared with plant cellulose, bacterial cellulose offers higher purity. Furthermore, the three-dimensional network structure formed during the secretion process enables a wider application with superior mechanical stability and excellent biocompatibility.

In this work, we report the fabrication of a flexible and scalable bacterial cellulose composite film (BCF) by embedding TiO_2 nanoparticles onto bacterial cellulose fibers and spraying a layer of polydimethylsiloxane (PDMS) on the surface for efficient and prolonged radiative cooling. The incorporation of TiO_2 as a composite filler improves the solar reflectance and photostability of bacterial cellulose. Benefiting from the multiple scattering effects of the porous structure, the BCF exhibits a considerable solar reflectivity of 89.1% and an infrared emissivity of 94.6%. Moreover, the BCF demonstrates excellent UV resistance, maintaining 88.1% of solar reflectance and 94.5% of infrared emissivity after 10 days of continuous UV exposure, thereby enabling sustained daytime radiative cooling. Outdoor performance tests reveal that the BCF achieves a maximum temperature drop of 7.15 °C when exposed under sunlight directly. Additionally, BCF possesses superior freshness retention capabilities, which can significantly

https://doi.org/10.1021/acsami.4c22615
ACS Appl. Mater. Interfaces 2025, 17, 6857−6866

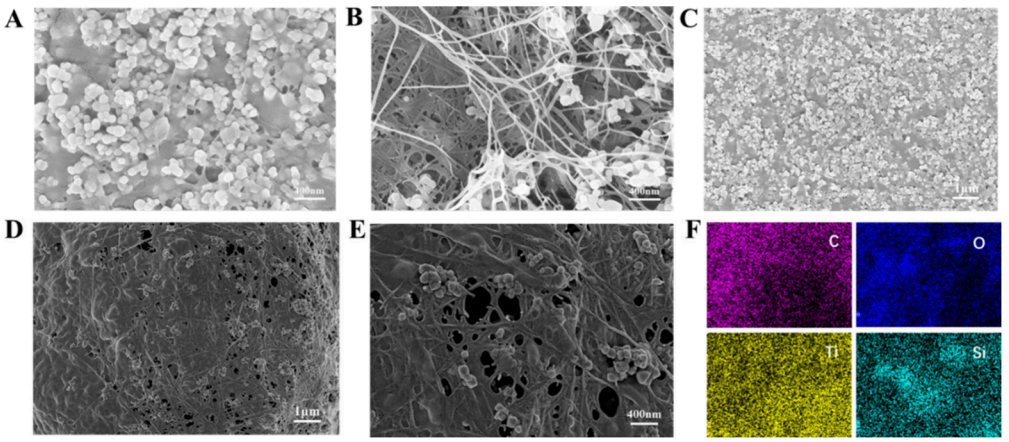

Figure 2. SEM images of the BCF: (A) SEM image of top sprayed PDMS; (B) SEM image of untreated bottom; (C, D) SEM images of the top and bottom BCF at scale bar of 1 μm, respectively, where the porous structure can be observed. (E) Magnified view of the lower surface; (F) EDS mapping of BCF.

slow down the dehydration rate of fruits. Therefore, the BCF exhibits enormous potential for applications in building energy conservation, cold chain packaging transportation, and solar cell temperature management.

RESULTS AND DISCUSSION

Design Strategy of BCF. To attain optimal results in radiative cooling, the following three essential criteria need to be satisfied: (1) high solar reflection in the solar band coupled with high infrared emission within the atmospheric transparent window; (2) development of mechanically robust and scalable radiative cooling materials to fulfill the demands of industrial or agricultural applications; (3) superior UV resistance to ensure prolonged radiative cooling performance under direct outdoor sunlight. The first criterion was addressed by employing biodegradable, dynamic bacterial cellulose as a substrate combined with TiO_2 nanoparticles. Bacterial cellulose exhibits significant infrared emission in the atmospheric transparency window due to the absorption vibrations of the characteristic molecular bonds of C−O−C and C−OH. In addition, the fiber structure of bacterial cellulose, which is comparable to the wavelength of sunlight, and the pore-like structure of the film formed during the drying process contribute to favorable solar reflectance. To meet the latter two requirements, TiO_2 nanoparticles were utilized to reinforce bacterial cellulose and promote UV resistance. Inherent absorption of TiO_2 in the UV region can prevent the photodegradation of the cellulose. Meanwhile, the solar reflectance was improved by incorporating TiO_2 nanoparticles, which are sized at ∼100 nm. As a result, the surface energy and surface area are greatly increased, thus improving the interaction with the surrounding environment. Consequently, in accordance with the above requirements, a flexible and scalable bacterial cellulose/TiO_2 composite film (BCF) was designed through a simple mixing and spraying method. As shown in Figure 1A, aqueous acrylic acid was added to bacterial cellulose and stirred to make a mixed solution. Meanwhile, TiO_2 was incorporated into a certain amount of deionized water and ultrasound for one h to prevent particle agglomeration. Then the ultrasounded homogeneous solution was mixed with the bacterial cellulose and stirred continuously for 2 h. The resulting white solution was cast onto a clean glass dish and dried for 24 h to form a bacterial cellulose film. Finally, a layer of PDMS was sprayed onto the film and dried at 80 °C for two h to obtain BCF (Figure 1B). The well-dispersed TiO_2 forms strong bonds with bacterial cellulose (C═O and O−Ti−O), creating a stable fiber network structure. Due to the absorption vibrations of the effective molecular bonds and pore structure in the composite system, the prepared BCF exhibits prominent solar reflectance and infrared emissivity. Compared with polymer-based materials (high-density polyethylene/boron nitride (HDPE/BN) and barium titanate nanorods/thermoplastic polyurethane (BST@TPU) membrane),[9,51] Figure 1C highlights the advantages of BCF in terms of biodegradability, UV resistance, and freshness, which can be used in numerous applications.

The Structure and Characterization of BCF. The morphology of BCF was observed by scanning electron microscopy (SEM), as shown in Figure 2A, displaying the top of the sprayed PDMS. Compared to the presprayed sample (Figure S1), most bacterial cellulose was covered by PDMS, but the fiber structure remained visible, and TiO_2 nanoparticles were not completely submerged and showed good dispersion due to the minimal content of sprayed PDMS, which formed only several molecular layers structure with the fibrous membrane. The bottom of the untreated fibrous membrane displayed an inter-cross-linked fiber network, and the TiO_2 nanoparticles were uniformly attached to the cellulose surface (Figure 2B). The agitation and drying process led to the formation of nanoscale pore-like structures on both sides of the membrane (Figure 2C and 2D), with sizes ranging from 100 to 400 nm (Figure 2E), promoting sunlight reflection. The membranes were further examined using energy dispersive spectroscopy (EDS), revealing the presence of Si elemental at the top surface of the sprayed PDMS (Figure 2F) while no Si element was detected at the bottom of the untreated surface (Figure S2).

The optical properties of the bacterial cellulose composite film were illustrated in Figure 3A. The bacterial cellulose membrane, characterized by its fibrous network structure, exhibits low absorption (10.9%) in the spectral range of 0.3−2.5 μm. The incorporation of TiO_2 not only improves the whiteness of the film but also suppresses the solar absorption rate, attributed to the strong light-scattering properties of TiO_2 nanoparticles. The low absorption rate can be attributed to three factors: (1) TiO_2 nanoparticles, with an average size of

https://doi.org/10.1021/acsami.4c22615
ACS Appl. Mater. Interfaces 2025, 17, 6857−6866

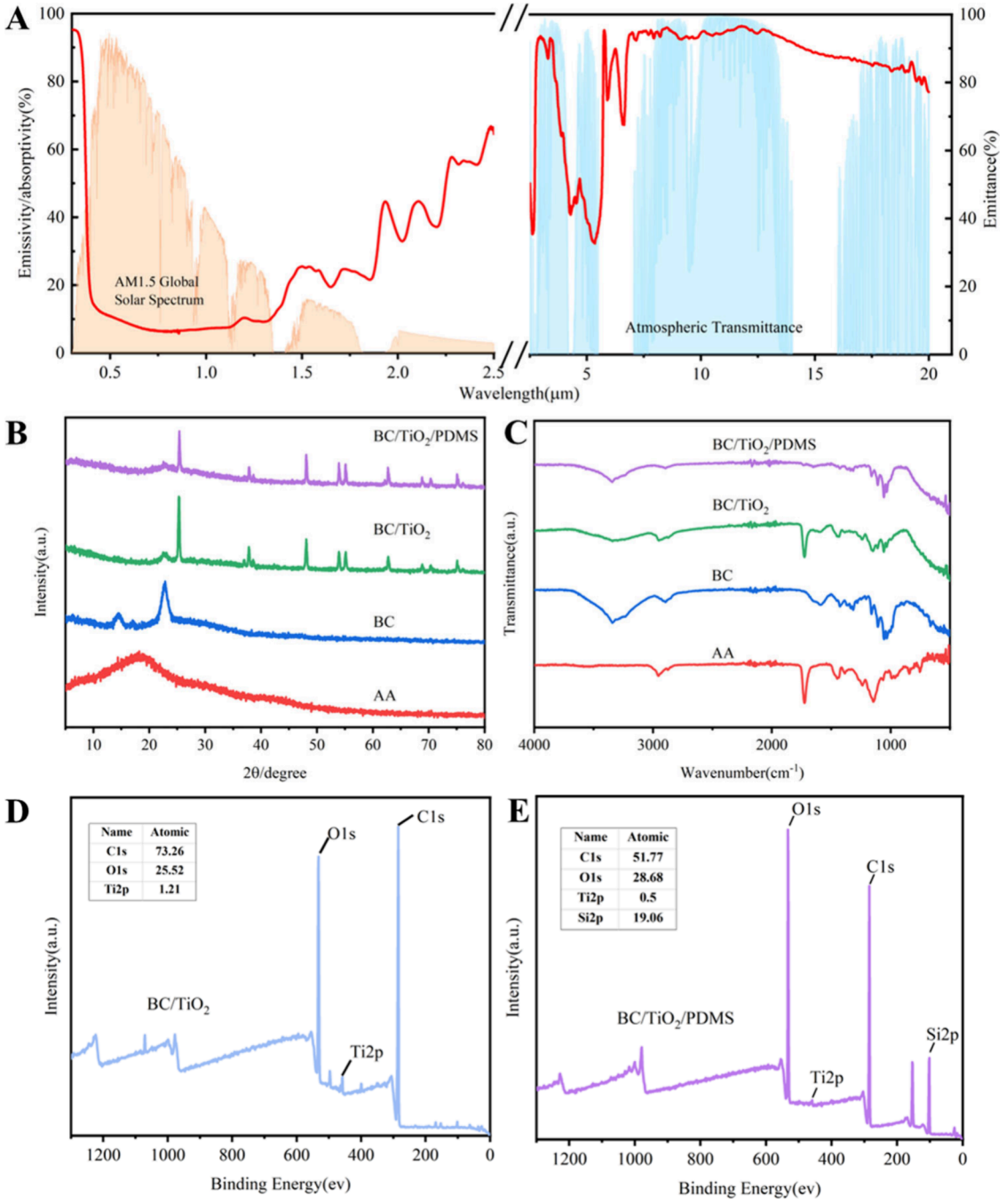

Figure 3. Optical properties and chemical structure of BCF: (A) spectral emittance of BCF from 0.3 to 20 μm, with the AM1.5 global solar spectrum and the realistic atmospheric transmittance model plotted for reference; (B, C) XRD patterns and FTIR spectra of AA, BC, BC/TiO_2, and BC/TiO_2/PDMS; (D) full XPS spectra of BC/TiO_2; (E) full XPS spectra of BC/TiO_2/PDMS.

100 nm, can enhance light scattering efficiency. (2) The fiber dimensions of bacterial cellulose are comparable to the sunlight wavelength and facilitated the scattering of sunlight. (3) The nanosized pore structure increases multiple scattering of BCF film, enabling broadband sunlight reflection. In addition to solar reflectance, infrared emissivity plays a key role in radiative cooling performance. As shown in the right side of Figure 3A, the BCF demonstrates an emissivity of 94.6% within the first atmospheric window (8−13 μm) and exhibits an emissivity of 84.6% in the second atmospheric window (16−20 μm). The high emissivity is primarily due to the vibrational absorption of C−O−C and C−OH bonds in bacterial cellulose and Si−O−Si bonds in PDMS. In addition, the thickness of the film significantly influences both the absorptivity and emissivity. As shown in Figures S3 and S4, as the thickness of the BCF increases, the polymer content increases, which leads to higher emissivity. When the thickness was raised from 1 to 20 μm, the emissivity increased substantially (from 68.2% to 88.7%), which could be caused by the decrease in transmittance. When the thickness is increased to 50 μm, the emissivity increases to 94.6%, and as the thickness continues to increase to 100 μm, the emissivity shows a decreasing trend from 94.6% to 94%. Despite the absorbance increase within the solar wavelength range, it still

https://doi.org/10.1021/acsami.4c22615
ACS Appl. Mater. Interfaces 2025, 17, 6857−6866

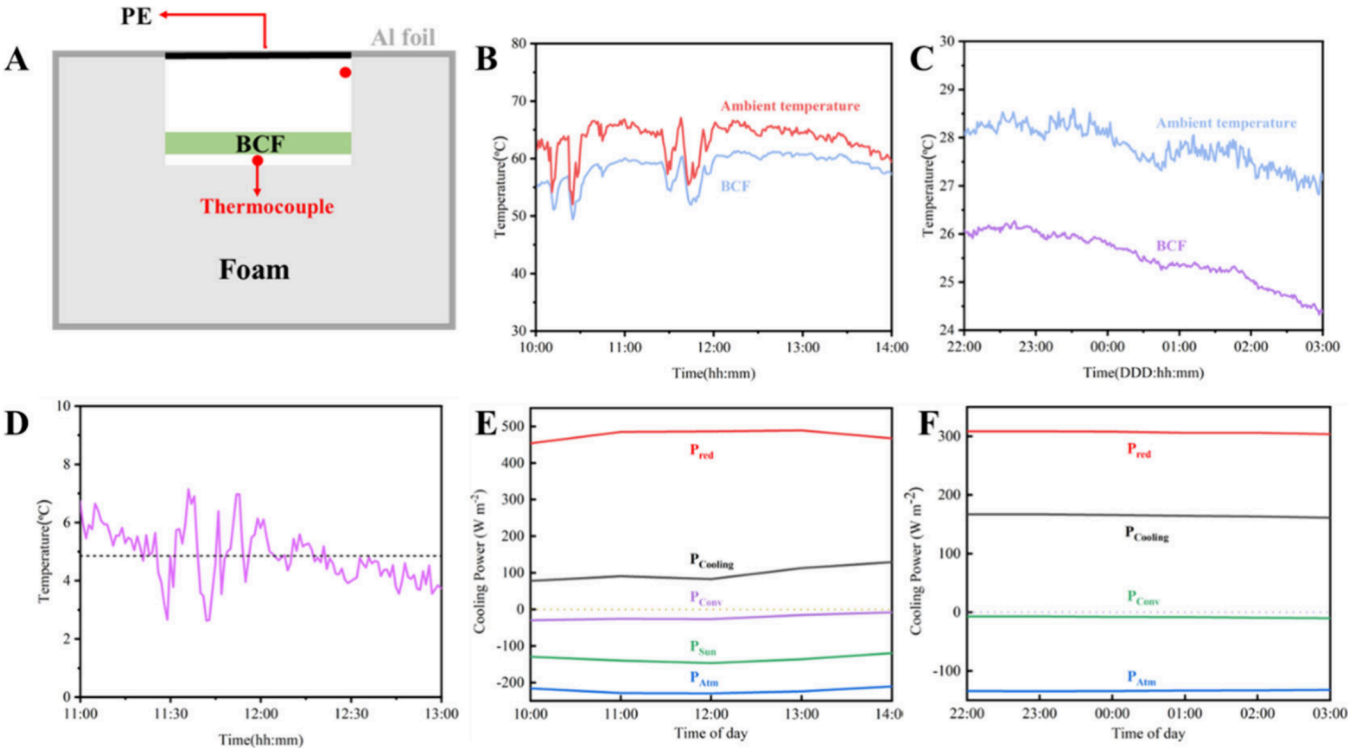

Figure 4. Daytime and nighttime radiative cooling performance of BCF: (A) schematic of the self-made device for outdoor tests of practical cooling performance of BCF; (B) comparison of the temperature changes measured with BCF and ambient air on July 4; (C) temperature changes in BCF and ambient air at night; (D) temperature difference between BCF and the ambient air; (E, F) cooling power ($P_{cooling}$) at (E) daytime and (F) nighttime.

has a low absorbance in the UV and visible range ($\alpha_{0.3\,\mu m\text{-}0.8\,\mu m}$ = 8.85%). In addition, we compared the reflectance and emissivity of TiO_2 for weight percentages of 0, 0.1, 1, 2, and 10 wt % (Figure S5). As the TiO_2 content gradually increases, the number of particles in the material that can participate in reflecting and scattering light increases and the reflectivity increases accordingly. So as the weight percent of TiO_2 increases from 0 wt % to 1 wt %, the reflectance increases from 56.2% to 89.1%. Although the addition of TiO_2 further improves reflectance, the improvement is not significant (2 wt %, 91.9%; 10 wt %, 92%). Moreover, a high content of TiO_2 will increase the thickness of the material, which will lead to a decrease in the flexibility of the film and limit its application in daily life. In addition, a high content of TiO_2 can significantly reduce the emissivity in the second atmospheric window (1 wt %, 84.6%; 2 wt %, 81.7%; 10 wt %, 77.9%). Compared with the slight increase in the first atmospheric window, it may result in a decrease in the overall emissivity. We also compared the IR emissivity and cooling performance with other reported cooling materials, such as dipentaerythritol pentahexaacrylate (DPHA) coating, cooling paper, and thermoplastic polyurethanes (TPU) membrane, the BCF showed higher IR emissivity and cooling efficiency, as shown in Table S1.

To elucidate the interactions among aqueous acrylic acid (AA), BC, TiO_2, and PDMS, XRD, FTIR, and XPS characterizations were conducted. Figure 3B presents the XRD patterns of pure AA, BC, BC/TiO_2, and BC/TiO_2/PDMS. Aqueous acrylic acid, a polymer composed of acrylate monomer-based vinyl monomer by emulsion polymerization, typically exhibits disordered molecular chains with low crystallinity, resulting in the absence of distinct diffraction peaks and an amorphous state in the XRD spectra. The characteristic peaks of BC appear at 14.8° and 24.2°, corresponding to the (110) and (200) crystal planes, respectively. The BC mixed with TiO_2 shows typical peaks of both BC and TiO_2. Due to the strong diffraction peaks of TiO_2 obscuring other BC peaks, the diffraction peaks of BC were indiscerning. Due to its amorphous structure, PDMS does not exhibit distinct diffraction peaks on the map. By comparison, PDMS-coated BC-TiO_2 hybrid membranes retained the crystal structure of TiO_2 and BC, indicating that the membranes were successfully encapsulated by PDMS without altering the crystal structure.

Figure 3C shows the FTIR spectra of pure AA, BC, BC/TiO_2, and BC/TiO_2/PDMS. Pure AA exhibits three characteristic peaks at 2957, 1725, and 1140 cm^{-1}, corresponding to the stretching vibration of C−H, C═O, and C−C, respectively. The FTIR spectrum of BC reveals distinct absorption peaks, with two strong C−O−C and C−O−H stretching vibrations near 1057 cm^{-1}, covering the molecular resonance range of 900−1200 cm^{-1}, which significantly contributes to the high emissivity within the atmospheric transparency window (8−13 μm, i.e., 770−1250 cm^{-1}). The strong absorption peak near 3351 cm^{-1} corresponds to the stretching vibration of the O−H group caused by intermolecular hydrogen bonding. Compared with the BC film, with the addition of TiO_2 and PDMS, BCF retains characteristic peaks of the BC film. Sprayed PDMS further increases the emissivity, because the molecular vibrations of Si-CH_3 and Si−O−Si are located within the atmospheric transparency window. Possibly due to the low content of AA, the typical characteristic peaks of AA cannot be identified.

To further investigate the interfacial interactions, X-ray photoelectron spectroscopy (XPS) experiments were per-

https://doi.org/10.1021/acsami.4c22615
ACS Appl. Mater. Interfaces 2025, 17, 6857−6866

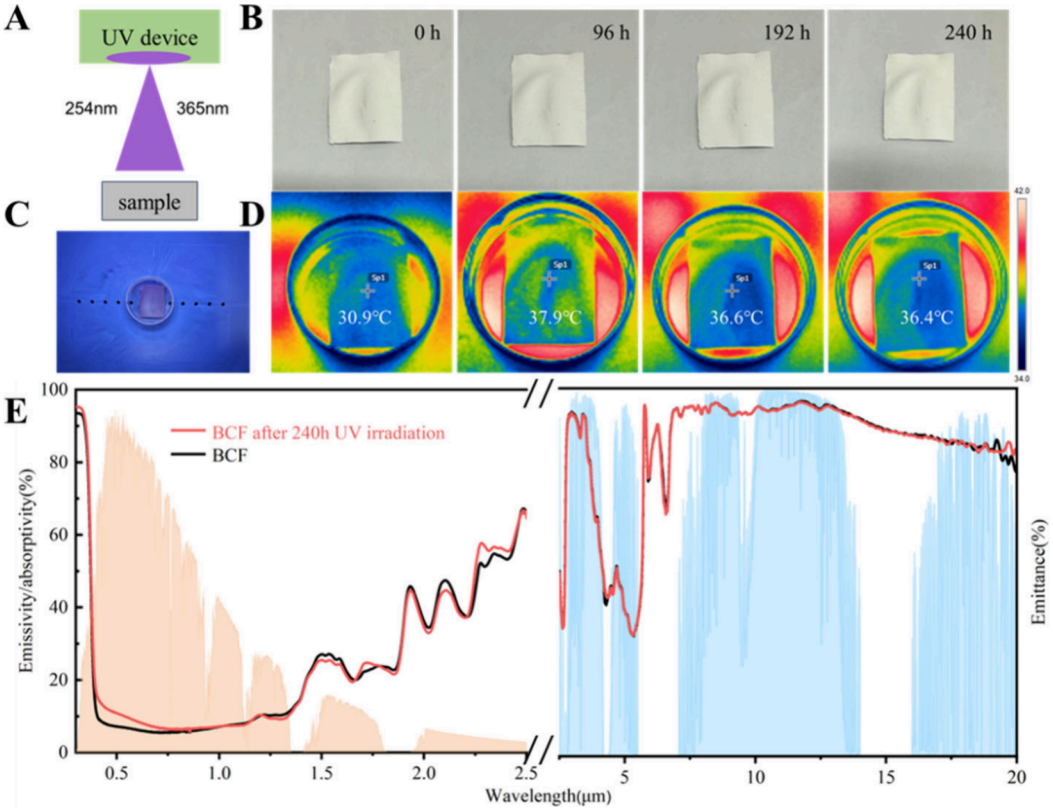

Figure 5. Sustainability of outdoor cooling performance: (A) schematic illustration of UV resistance test; (B) photographs of BCF under UV light at different times; (C) images of BCF in the UV chamber; (D) IR mages of BCF under UV light; (E) spectral emittance of BCF (initial) and BCF (240 h of UV irradiation).

formed on BC, BC/TiO_2, and BC/TiO_2/PDMS membranes (Figure S6). The XPS spectrum of BC exhibited only two peaks, corresponding to the C 1s and O 1s orbitals. For BC/TiO_2, the characteristic peaks at binding energies of 284.8, 532.39, and 458.43 eV corresponded to the C 1s, O 1s, and Ti 2p electronic orbits, respectively (Figure 3D). The XPS spectrum of BC/TiO_2/PDMS also displayed peaks for C 1s, O 1s, and Ti 2p electronic orbits, appearing at 284.8, 532.46, and 458.93 eV, respectively (Figure 3E). In addition, a characteristic peak of Si appears at 102.33 eV, indicating the successful incorporation of PDMS into the BC/TiO_2 matrix. Detailed analyses of the Ti 2p spectra for BC/TiO_2 and Ti 2p and Si 2p spectra for BC/TiO_2/PDMS revealed that the energy difference between spin−orbit peaks Ti $2p_{1/2}$ and Ti $2p_{3/2}$ was 5.55 eV (Figure S7), which is consistent with Ti^{4+} oxidation state in the TiO_2 lattice.[52] Fitting the data, the full width at half-maximum (fwhm) values for Ti $2p_{3/2}$ and Ti 2p were determined to be 1.06 and 1.74, respectively. After spraying PDMS, the binding energies of Ti $2p_{1/2}$ and Ti $2p_{3/2}$ in BC/TiO_2/PDMS shifted to 458.93 and 464.51 eV, respectively (Figure S8 left). The Si 2p spectrum of BC/TiO_2/PDMS exhibited two binding energy peaks at 102.22 and 102.89 eV, corresponding to Si−OH and Si−O bonds, respectively (Figure S8 right).

Radiative Cooling Performance of BCF. To evaluate the cooling potential of the BCF, its radiative cooling performance was tested on the rooftop in Nanjing (July 4, 2024, the outdoor temperature is 36 °C and the relative humidity is 53%) by using a self-made device (the schematic and device diagrams as shown in Figure 4A and Figure S9). The device comprised polystyrene foam covered with an aluminum foil to mitigate the ambient temperature interference. A high-precision type K thermocouple was affixed to the bottom of the BCF, while another type K thermocouple was positioned at the interior wall for comparative purposes, and a multichannel temperature recorder was used to record real-time temperatures. Finally, a polyethylene film was employed on top of the device to inhibit heat convection. As shown in Figure 4B, during the interval from 11:00 a.m. to 1:00 p.m., the temperature below the BCF was substantial reduced relative to the ambient temperature, with a maximum decrement of 7.15 °C around 11:30 a.m. under direct sunlight, and an average temperature reduction of 4.85 °C (Figure 4D). Meanwhile, to evaluate the nighttime radiative cooling performance of the BCF, the temperatures of real-time nighttime from 10:00 p.m. to 3:00 a.m. (next day) were recorded. As shown in Figure 4C, the temperatures of the BCF remained below ambient, with an average reduction of 2.32 °C. We calculated the cooling power of the BCF during the day and night. Calculation of the cooling power is shown in eqs 4−15 of the Supporting Information. As shown in Figure 4E,F, the average cooling power during the daytime from 10:00 a.m. to 2:00 p.m. is 98.7 W m^{-2}. And there is a tendency for the cooling power to decrease due to the increase in solar intensity at noon and the increase in temperature resulting in a rise in P_{sun} and $P_{cond+conv}$. However, the cooling power can still reach 83 W m^{-2}. Similarly, theoretical calculations yielded an average cooling power of 164.7 W m^{-2} at night; since there is no solar radiative as a source of heat input at night, the heat received by the BCF comes only from thermal radiation and heat transfer from the surrounding environment, resulting in a higher cooling power at night than during the daytime. In addition,

https://doi.org/10.1021/acsami.4c22615
ACS Appl. Mater. Interfaces 2025, 17, 6857−6866

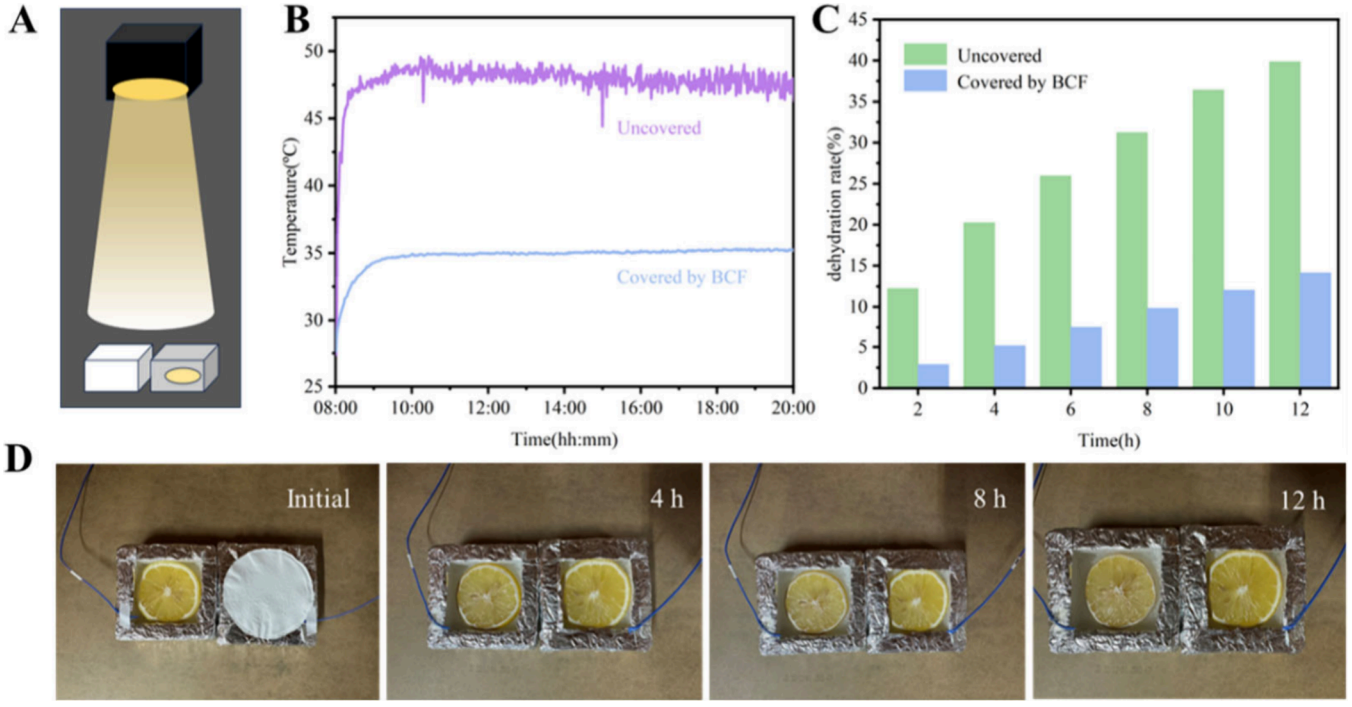

Figure 6. Application in fruit preservation: (A) schematic diagram of simulated daylight exposure; (B) comparison of temperature changes measured with covered BCF and exposed to the light source; (C) simulating the dehydration rate of lemons under sunlight; (D) changes in the appearance of lemons under simulated sunlight.

comparisons of the daytime and nighttime temperatures of BCF and the ground surface in Figure S10A,B revealed average cooling rates of 6.48 and 6.92 °C, respectively (Figure S10C,D). We also measured the radiative cooling performance of the BCF in different weather, to ensure that both thermocouples are exposed to sunlight at the same time, the entire unit is tilted 45° toward the south. As shown in Figure S11, on sunny and cloudy days, the temperatures of BCF were on average 5.04 and 4 °C lower than ambient temperatures, respectively. Besides, we present Table S2 to compare reflectance, emissivity, and temperature difference for recently reported materials in the field of radiative cooling. The advantages of the BCF's outdoor cooling capacity are obvious.

UV Resistance Test. As a biopolymer, bacterial cellulose is vulnerable to UV radiation when exposed to outdoor environments. The high energy of UV light is capable of triggering free radical reactions in polymers, leading to the breakdown of chemical bonds and accelerating polymer aging. Moreover, exposure to UV light causes the polymer to change color while reducing its strength and toughness, rendering it brittle. Therefore, the long-term stability of BCF under outdoor conditions is critical for practical applications. To evaluate the UV resistance of BCF, it was subjected to a UV chamber with two specific wavelengths (254 and 365 nm); schematic and test diagrams are shown in Figure 5A,C. Throughout the UV exposure period from 0 to 96 h, the BCF maintained its appearance without significant color change. Even after 192 h irradiation, the BCF retained its ultrawhite appearance (Figure 5B). Infrared thermography was also employed to monitor the surface temperature of the BCF. As shown in Figure 5D, the temperature of the BCF increased by 7 °C after a short period of irradiation (96 h). While after a long period of irradiation of 240 h, the surface temperature of the BCF showed a decreasing trend and was significantly lower than the surrounding temperature, demonstrating its long-term solar reflectance properties. This is confirmed by the solar absorptivity and infrared emissivity in Figure 5E, which indicate minimal changes in these parameters even after 240 h of UV irradiation.

As a flexible, scalable device for outdoor use, the BCF needs to adapt to a variety of environments and weather. Therefore, BCF needs to be hydrophobic and durable, and the surface of BCF is hydrophobic due to the sprayed layer of PDMS. As shown in Figure S12, as evidenced by an increased CA from 55° to 86°. For the mechanical properties, the BCF with a thickness of 1 μm has a tensile strength of 6 MPa and an elongation rate of 1.26%. When the thickness is increased to 20 μm, the tensile strength and elongation at break are increased to 28 MPa and 3.21% respectively. The obtained BCF with a thickness of 50 μm retains its flexibility, whereas its tensile strength and elongation rate in the axial direction is improved by 40 MPa and 4.45% (Figure S13), which is sufficient to cope with the dust and complex weather of daily life.

Fruit Preservation of BCF. To evaluate the efficiency of the bacterial cellulose composite film in preserving fruit freshness, lemons were employed as the model fruits. Two lemons of comparable sizes (Figure S14) were placed in uncovered and BCF-covered expanded polyethylene (EPE) containers with the exterior wrapped with aluminum foil, respectively. The fruits were then exposed to simulated daylight by a xenon lamp as the schematic diagram is shown in Figure 6A. Multiplexed temperature recorder with type K thermocouples was used to record the real-time temperature of two lemons. Ambient temperature and humidity were monitored with the corresponding temperature and humidity loggers. At an average temperature and humidity of 26.8 °C and 56%, respectively (Figure S15), the temperature of the fruits with BCF-covered increased more gradually than that

https://doi.org/10.1021/acsami.4c22615
ACS Appl. Mater. Interfaces 2025, 17, 6857−6866

without BDF coating, demonstrating superior cooling effects, with a maximum observed cooling of 14.7 °C (Figure 6B). To further evaluate the freshness retention effect of BCF, their dehydration rate was recorded and calculated in comparison to the initial weights every two h by means of a balance. (Calculation of the dehydration rate is shown in eq 3 of the Supporting Information). Lemons in BCF-covered containers exhibited considerably lower dehydration rates compared with those in uncovered containers (Figure 6C). In addition, lemons were observed every 4 h for changes in appearance, and lemons in uncovered containers rapidly lost water and wilted after 12 h of continuous exposure. Remarkably, even after 12 h of exposure, the BCF-covered lemons showed no significant dehydration or structural shrinkage (Figure 6D). To better demonstrate the preservation effect of BCF, we compared the temperature and dehydration rate of lemons covered with different materials, including uncovered, weighing paper, PE, and BCF covered. As shown in Figure S16A,B, lemons in BCF-covered containers exhibited considerably lower dehydration rates compared to the other three lemons. Even after 12 h of exposure, the dehydration rate of BCF-covered lemons was only 9.1%, compared to uncovered (36.7%), weighing paper (29.4%), and PE (17.7%), the BCF demonstrates superior freshness effects, and the temperature of the BCF-covered containers was much lower than that of the weighing paper and PE film coverings. In terms of appearance, uncovered, weighing paper, and PE covered lemons had varying degrees of dehydration and wrinkling, while BCF-covered lemons had no apparent structural shrinkage (Figure S17).

CONCLUSION

We have successfully engineered a biobased BCF with a cross-linked network architecture through a straightforward agitation spraying technique, achieving enhanced functionality and environmentally sustainable radiative cooling properties. The integration of TiO_2 nanoparticles and PDMS as composite fillers significantly augmented the solar reflectance, infrared emissivity, and durability of the bacterial cellulose matrix. Moreover, the intrinsic fiber and pore structure facilitated multiple scattering, resulting in a high solar reflection of 89.1%, a high infrared emissivity of 94.6%, and exceptional UV resistance. Remarkably, after 240 h of continuous UV exposure, the BCF's surface temperature and optical properties remained largely unaltered. Additionally, the BCF exhibited excellent efficacy in maintaining the freshness of fruits. The BCF demonstrates significant potential applications in building energy conservation, photovoltaic systems, and food packaging for transportation.

MATERIALS AND METHODS

Materials. Bacterial cellulose was purchased from ScienceK Co., Ltd. Titanium dioxide (TiO_2) nanoparticles (particle size = 100 nm) were purchased from Shanghai Macklin Biochemical Co., Ltd. Aqueous acrylic acid (AA) were supplied by Anhui Dizhi Chemical Technology Co., Ltd. Polydimethylsiloxane (PDMS) was purchased from Dow Corning Co., Ltd. Cyclohexane was purchased from Shanghai Titan Scientific Co., Ltd.

Preparation of BC/TiO_2 Composite Film (BCF). First, 0.1 mL of aqueous acrylic acid and 20 mL of bacterial cellulose were added into a 100 mL beaker and stirred at 400 rpm for 1h to form a homogeneous solution. Meanwhile, 0.2 g of TiO_2 (1 wt %) was placed in a beaker containing 10 mL of deionized water and sonicated for 1 h to prevent agglomeration of particles. The sonicated TiO_2 was poured into the mixture of bacterial cellulose and aqueous acrylic acid and continued to be stirred for 2 h. Finally, the stirred solution is coated on the glass plate and dried naturally for 12 h. Four g of PDMS was added to 16 mL of cyclohexane, diluted five times, and then sprayed onto the film using a commercial spray gun and dried in an oven at 80 °C for 2 h to cure. After curing, the film can be easily removed from the glass plate to get the BC/TiO_2 composite film (BCF).

Characterization. The morphologic structure of BCF was evaluated by using a field emission scanning electron microscope (Gemini 300). The solar absorption of BCF (0.3−2.5 μm) was measured using a UV−vis−NIR spectrophotometer (Lambda950, PerkinElmer) equipped with an integrating sphere model. Infrared emissivity (2.5−20 μm) of BCF were tested by using a Fourier transform infrared spectrometer (Nicolet 6700, Thermo Fisher Scientific) equipped with a gold integrating sphere. The IR images were recorded by monitoring the temperatures of BCF with an IR camera (FLIR E40). Chemical structure of BCF was evaluated using Fourier transform infrared spectroscopy (Nicolet iS20 FTIR, Thermo Fisher Scientific). The outdoor radiative cooling performance of BCF was tested at Nanjing University of Information Science & Technology (China). A piece of BCF placed into a self-made polystyrene foam box (30 cm × 30 cm × 30 cm) was used for testing. Thermocouples were used to measure the temperature changes of the BCF and the ambient air near the experimental setup. The BCF was placed in a UV chamber with wavelengths of 254 and 365 nm for 240 h of continuous irradiation to evaluate its long-term stability.

ASSOCIATED CONTENT

Data Availability Statement

The data that support the findings of this study are available from the corresponding author upon reasonable request.

Supporting Information

The Supporting Information is available free of charge at https://pubs.acs.org/doi/10.1021/acsami.4c22615.

Photograph and scanning electron microscopy of BCF before PDMS spraying; elemental mapping at the bottom of the BCF; reflectance and emissivity of different ratios of TiO_2 and different thicknesses of BCF; XPS spectra of BC, BC/TiO_2, and BC/TiO_2/PDMS; temperature differences between the BCF and air on October 29, 2024 (sunny) and November 13, 2024 (cloudy); stress−strain curves of BCF with different thicknesses; dehydration rate of uncovered, weighing paper, PE and BCF covered lemons after 12 h of continuous irradiation (PDF)

AUTHOR INFORMATION

Corresponding Author

Hao-Yu Zhao − *School of Chemistry and Materials Science, Jiangsu Key Laboratory of New Energy Devices & Interface Science, Nanjing University of Information Science & Technology, Nanjing 210026, China; School of Environmental Science and Engineering, Jiangsu Key Laboratory of Atmospheric Environment Monitoring and Pollution Control, Nanjing University of Information Science & Technology, Nanjing 210026, China;* orcid.org/0000-0002-2648-271X; Email: haoyuzhao@nuist.edu.cn

Authors

Yuan-Cheng Ding − *School of Chemistry and Materials Science, Jiangsu Key Laboratory of New Energy Devices & Interface Science, Nanjing University of Information Science & Technology, Nanjing 210026, China*

Guo-Wei Tang − *Department of Energy and Resources Engineering, College of Engineering, Peking University, Beijing 100871, China;* orcid.org/0009-0006-1583-9273

https://doi.org/10.1021/acsami.4c22615
ACS Appl. Mater. Interfaces 2025, 17, 6857−6866

Jia-Ming Liu − *School of Chemistry and Materials Science, Jiangsu Key Laboratory of New Energy Devices & Interface Science, Nanjing University of Information Science & Technology, Nanjing 210026, China*
Tian-Hao Fan − *School of Chemistry and Materials Science, Jiangsu Key Laboratory of New Energy Devices & Interface Science, Nanjing University of Information Science & Technology, Nanjing 210026, China*
Yu-Can Peng − *Department of Energy and Resources Engineering, College of Engineering, Peking University, Beijing 100871, China*
Pin Jern Ker − *School of Engineering and Technology, Sunway University, Petaling Jaya 47500, Malaysia*
Dong-Sheng Geng − *School of Chemistry and Materials Science, Jiangsu Key Laboratory of New Energy Devices & Interface Science, Nanjing University of Information Science & Technology, Nanjing 210026, China; School of Materials Science and Engineering, University of Science and Technology Beijing, Beijing 100083, P. R. China;* orcid.org/0000-0003-0910-8985

Complete contact information is available at: https://pubs.acs.org/10.1021/acsami.4c22615

Author Contributions

†Yuan-Cheng Ding and Guo-Wei Tang contributed equally to this work. Y.-C.D. and G.-W.T. contributed equally to this work. H.-Y.Z., Y.-C.D., and D.-S.G. conceived the idea and designed the research project. H.-Y.Z., Y.-C.D., and G.-W.T. performed the experiments. H.-Y.Z., Y.-C.D., J.-M.L., and T.-H.F. collected and analyzed the data. Y.-C.D. and H.-Y.Z. wrote the manuscript. H.-Y.Z., Y.-C.P., and P.J.K. supervised the project. All of the authors discussed the results and commented on the manuscript.

Notes

The authors declare no competing financial interest.

■ ACKNOWLEDGMENTS

This work was supported by the National Natural Science Foundation of China (Grant 22105196), Start-up Fee for the Construction and Development of Higher Education in Jiangsu Province (Grant 2023r034), and China Postdoctoral Science Foundation (Grant 2023M731753).

■ REFERENCES

(1) Huang, M.-T.; Zhai, P.-M. Achieving Paris Agreement temperature goals requires carbon neutrality by middle century with far-reaching transitions in the whole society. *Advances in Climate Change Research* **2021**, *12* (2), 281−286.
(2) Ke, Y.; Chen, J.; Lin, G.; Wang, S.; Zhou, Y.; Yin, J.; Lee, P. S.; Long, Y. Smart Windows: Electro-, Thermo-, Mechano-, Photochromics, and Beyond. *Adv. Energy Mater.* **2019**, *9* (39), 1902066.
(3) Wu, X.; Li, J.; Xie, F.; Wu, X.-E.; Zhao, S.; Jiang, Q.; Zhang, S.; Wang, B.; Li, Y.; Gao, D.; Li, R.; Wang, F.; Huang, Y.; Zhao, Y.; Zhang, Y.; Li, W.; Zhu, J.; Zhang, R. A dual-selective thermal emitter with enhanced subambient radiative cooling performance. *Nat. Commun.* **2024**, *15* (1), 815.
(4) Li, W.; Zhan, H.; Huang, N.; Ying, Y.; Yu, J.; Zheng, J.; Qiao, L.; Li, J.; Che, S. Scalable and Flexible Multi-Layer Prismatic Photonic Metamaterial Film for Efficient Daytime Radiative Cooling. *Small Methods* **2024**, *8* (7), 2301258.
(5) Wang, C.; Chen, H.; Wang, F. Passive daytime radiative cooling materials toward real-world applications. *Prog. Mater. Sci.* **2024**, *144*, 101276.
(6) Raman, A. P.; Anoma, M. A.; Zhu, L.; Rephaeli, E.; Fan, S. Passive radiative cooling below ambient air temperature under direct sunlight. *Nature* **2014**, *515* (7528), 540−544.
(7) Li, W.; Dong, M.; Fan, L.; John, J. J.; Chen, Z.; Fan, S. Nighttime Radiative Cooling for Water Harvesting from Solar Panels. *ACS Photonics* **2021**, *8* (1), 269−275.
(8) Zhao, B.; Hu, M.; Ao, X.; Chen, N.; Xuan, Q.; Jiao, D.; Pei, G. Performance analysis of a hybrid system combining photovoltaic and nighttime radiative cooling. *Applied Energy* **2019**, *252*, 113432.
(9) Zhang, W.; Wang, Y.; Sun, H.; Liu, C.; Shen, C.; Liu, X. Thermal conductive high-density polyethylene/boron nitride composites with high solar reflectivity for radiative cooling. *Adv. Compos. Hybrid Mater.* **2023**, *6* (5), 163.
(10) Yang, Z.; Jia, Y.; Zhang, J. Hierarchical-Morphology Metal/Polymer Heterostructure for Scalable Multimodal Thermal Management. *ACS Appl. Mater. Interfaces* **2022**, *14* (21), 24755−24765.
(11) Xu, F.; Wang, F.; Ou, J. Superhydrophobic polytetrafluoroethylene/polyvinylidene fluoride coating for passive daytime radiative refrigeration. *Colloids Surf., A* **2023**, *676*, 132121.
(12) Yang, Y.; Li, X.; Zhou, Z.; Qiu, Q.; Chen, W.; Huang, J.; Cai, W.; Qin, X.; Lai, Y. Ultrathin, ultralight dual-scale fibrous networks with high-infrared transmittance for high-performance, comfortable and sustainable PM0.3 filter. *Nat. Commun.* **2024**, *15* (1), 1586.
(13) Zhang, Q.; Qi, C.; Wang, X.; Zhu, B.; Li, W.; Xiao, X.; Fu, H.; Hu, S.; Zhu, S.; Xu, W.; Zhu, J. Daytime radiative cooling dressings for accelerating wound healing under sunlight. *Nature Chemical Engineering* **2024**, *1* (4), 301−310.
(14) Zhou, L.; Song, H.; Liang, J.; Singer, M.; Zhou, M.; Stegenburgs, E.; Zhang, N.; Xu, C.; Ng, T.; Yu, Z.; Ooi, B.; Gan, Q. A polydimethylsiloxane-coated metal structure for all-day radiative cooling. *Nature Sustainability* **2019**, *2* (8), 718−724.
(15) Choi, M.; Seo, J.; Yoon, S.; Nam, Y.; Lee, J.; Lee, B. J. All-day radiative cooling using a grating-patterned PDMS film emitter. *Applied Thermal Engineering* **2022**, *214*, 118771.
(16) Min, X.; Wang, X.; Li, J.; Xu, N.; Du, X.; Zeng, M.; Li, W.; Zhu, B.; Zhu, J. A smart thermal-gated bilayer membrane for temperature-adaptive radiative cooling and solar heating. *Science Bulletin* **2023**, *68* (18), 2054−2062.
(17) Fan, W.; Gao, Q.; Xiang, J.; Yan, J.; Chen, Y.; Fan, H. Synergistic effect of silica aerogel and titanium dioxide in porous polyurethane composite coating with enhanced passive radiative cooling performance. *Prog. Org. Coat.* **2023**, *183*, 107763.
(18) Li, M.; Zhang, M.; Mahar, F. K.; Wei, L.; Wang, Z.; Wang, X.; Wei, K. Fabrication of fibrous nanofiber membranes for passive radiation cooling. *J. Mater. Sci.* **2022**, *57* (33), 16080−16090.
(19) Huang, Z.; Ruan, X. Nanoparticle embedded double-layer coating for daytime radiative cooling. *Int. J. Heat Mass Transfer* **2017**, *104*, 890−896.
(20) Fu, Y.; Yang, J.; Su, Y. S.; Du, W.; Ma, Y. G. Daytime passive radiative cooler using porous alumina. *Sol. Energy Mater. Sol. Cells* **2019**, *191*, 50−54.
(21) Xiang, B.; Zhang, R.; Luo, Y.; Zhang, S.; Xu, L.; Min, H.; Tang, S.; Meng, X. 3D porous polymer film with designed pore architecture and auto-deposited SiO_2 for highly efficient passive radiative cooling. *Nano Energy* **2021**, *81*, 105600.
(22) Hu, W.; Zhang, F.; Tan, X.; Tu, Y.; Nie, S. Antibacterial PVDF Coral-Like Hierarchical Structure Composite Film Fabrication for Self-Cleaning and Radiative Cooling Effect. *ACS Appl. Mater. Interfaces* **2024**, *16* (15), 19828−19837.
(23) Yang, Z.; Zhang, J. Bioinspired Radiative Cooling Structure with Randomly Stacked Fibers for Efficient All-Day Passive Cooling. *ACS Appl. Mater. Interfaces* **2021**, *13* (36), 43387−43395.
(24) Zhang, H.; Ly, K. C. S.; Liu, X.; Chen, Z.; Yan, M.; Wu, Z.; Wang, X.; Zheng, Y.; Zhou, H.; Fan, T. Biologically inspired flexible photonic films for efficient passive radiative cooling. *Proc. Natl. Acad. Sci. U. S. A.* **2020**, *117* (26), 14657−14666.
(25) Lin, K.; Chen, S.; Zeng, Y.; Ho, T. C.; Zhu, Y.; Wang, X.; Liu, F.; Huang, B.; Chao, C. Y.-H.; Wang, Z.; Tso, C. Y. Hierarchically

structured passive radiative cooling ceramic with high solar reflectivity. *Science* **2023**, *382* (6671), 691−697.
(26) Li, T.; Sun, H.; Yang, M.; Zhang, C.; Lv, S.; Li, B.; Chen, L.; Sun, D. All-Ceramic, compressible and scalable nanofibrous aerogels for subambient daytime radiative cooling. *Chemical Engineering Journal* **2023**, *452*, 139518.
(27) Cai, C.; Wei, Z.; Ding, C.; Sun, B.; Chen, W.; Gerhard, C.; Nimerovsky, E.; Fu, Y.; Zhang, K. Dynamically Tunable All-Weather Daytime Cellulose Aerogel Radiative Supercooler for Energy-Saving Building. *Nano Lett.* **2022**, *22* (10), 4106−4114.
(28) Ma, J.-W.; Zeng, F.-R.; Lin, X.-C.; Wang, Y.-Q.; Ma, Y.-H.; Jia, X.-X.; Zhang, J.-C.; Liu, B.-W.; Wang, Y.-Z.; Zhao, H.-B. A photoluminescent hydrogen-bonded biomass aerogel for sustainable radiative cooling. *Science* **2024**, *385* (6704), 68−74.
(29) Zhang, Q.; Xue, T.; Lu, Y.; Ma, L.; Yu, D.; Liu, T.; Fan, W. Fluorine-containing polyimide nanofiber membranes for durable and anti-aging daytime radiative cooling. *Journal of Materials Science & Technology* **2024**, *179*, 166−173.
(30) Wang, J.; Sun, J.; Guo, T.; Zhang, H.; Xie, M.; Yang, J.; Jiang, X.; Chu, Z.; Liu, D.; Bai, S. High-Strength Flexible Membrane with Rational Pore Architecture as a Selective Radiator for High-Efficiency Daytime Radiative Cooling. *Adv. Mater. Technol.* **2022**, *7* (1), 2100528.
(31) Xie, B.; Liao, H.; Tu, H.; Mei, J.; Hou, M.; Wang, J. "Sandwich Structured" Composite Film with Double Barrier Radiative Cooling, Adjustable Heating, and Multi-reflective Electromagnetic Interference Shielding for All-Weather Protection. *ACS Photonics* **2024**, *11* (11), 5039−5049.
(32) Yan, Z.; Zhai, H.; Fan, D.; Li, Q. A trimode textile designed with hierarchical core-shell nanofiber structure for all-weather radiative personal thermal management. *Nano Today* **2023**, *51*, 101897.
(33) Xue, S.; Huang, G.; Chen, Q.; Wang, X.; Fan, J.; Shou, D. Personal Thermal Management by Radiative Cooling and Heating. *Nano-Micro Lett.* **2024**, *16* (1), 153.
(34) Lan, C.; Xu, F.; Pan, C.; Hao Guo, Z.; Pu, X. MXene based Janus fabrics with radiative heating towards efficient personal thermal management. *Chemical Engineering Journal* **2023**, *472*, 144662.
(35) Dai, B.; Li, X.; Xu, T.; Zhang, X. Radiative Cooling and Solar Heating Janus Films for Personal Thermal Management. *ACS Appl. Mater. Interfaces* **2022**, *14* (16), 18877−18883.
(36) Li, X.; Dai, B.; Wang, L.; Yang, X.; Xu, T.; Zhang, X. Radiative cooling and anisotropic wettability in E-textile for comfortable biofluid monitoring. *Biosens. Bioelectron.* **2023**, *237*, 115434.
(37) Hu, X.; Tian, M.; Xu, T.; Sun, X.; Sun, B.; Sun, C.; Liu, X.; Zhang, X.; Qu, L. Multiscale Disordered Porous Fibers for Self-Sensing and Self-Cooling Integrated Smart Sportswear. *ACS Nano* **2020**, *14* (1), 559−567.
(38) Li, S.; Zhou, Z.; Liu, J.; Zhang, J.; Tang, H.; Zhang, Z.; Na, Y.; Jiang, C. Research on indirect cooling for photovoltaic panels based on radiative cooling. *Renewable Energy* **2022**, *198*, 947−959.
(39) Hu, X.; Wang, S.; Feng, R.; Hu, K. Natural organic small molecules promote the aging of plastic wastes and refractory carbon decomposition in water. *Journal of Hazardous Materials* **2024**, *469*, 134043.
(40) Wang, H.; Zhou, Q. Bioelectrochemical systems - A potentially effective technology for mitigating microplastic contamination in wastewater. *Journal of Cleaner Production* **2024**, *450*, 141931.
(41) Pedersen, G. B.; Blaschek, L.; Frandsen, K. E. H.; Noack, L. C.; Persson, S. Cellulose synthesis in land plants. *Molecular Plant* **2023**, *16* (1), 206−231.
(42) Bahloul, A.; Kassab, Z.; El Bouchti, M.; Hannache, H.; Qaiss, A. E. K.; Oumam, M.; El Achaby, M. Micro- and nano-structures of cellulose from eggplant plant (Solanum melongena L) agricultural residue. *Carbohydr. Polym.* **2021**, *253*, 117311.
(43) Ramírez-Rodríguez, E. A.; McFarlane, H. E. Insights from the Structure of a Plant Cellulose Synthase Trimer. *Trends in Plant Science* **2021**, *26* (1), 4−7.
(44) Santos, D. A.; Oliveira, M. M.; Curvelo, A. A. S.; Fonseca, L. P.; Porto, A. L. M. Hydrolysis of cellulose from sugarcane bagasse by cellulases from marine-derived fungi strains. *International Biodeterioration & Biodegradation* **2017**, *121*, 66−78.
(45) Rühs, P. A.; Malollari, K. G.; Binelli, M. R.; Crockett, R.; Balkenende, D. W. R.; Studart, A. R.; Messersmith, P. B. Conformal Bacterial Cellulose Coatings as Lubricious Surfaces. *ACS Nano* **2020**, *14* (4), 3885−3895.
(46) Chen, C.; Ding, W.; Zhang, H.; Zhang, L.; Huang, Y.; Fan, M.; Yang, J.; Sun, D. Bacterial cellulose-based biomaterials: From fabrication to application. *Carbohydr. Polym.* **2022**, *278*, 118995.
(47) Zhu, W.; Droguet, B.; Shen, Q.; Zhang, Y.; Parton, T. G.; Shan, X.; Parker, R. M.; De Volder, M. F. L.; Deng, T.; Vignolini, S.; Li, T. Structurally Colored Radiative Cooling Cellulosic Films. *Adv. Sci.* **2022**, *9* (26), 2202061.
(48) Cai, C.; Chen, F.; Wei, Z.; Ding, C.; Chen, Y.; Wang, Y.; Fu, Y. Large scalable, anti-ultraviolet, strong cellulose film with well-defined dual-pores for longtime daytime radiative cooling. *Chemical Engineering Journal* **2023**, *476*, 146668.
(49) Chen, Y.; Dang, B.; Fu, J.; Wang, C.; Li, C.; Sun, Q.; Li, H. Cellulose-Based Hybrid Structural Material for Radiative Cooling. *Nano Lett.* **2021**, *21* (1), 397−404.
(50) Wang, Q.; Zhong, S.; Zheng, Z.; Lei, H.; Li, S.; Yu, W. Bacterial cellulose based three-dimensional porous composites with remarkable amphiphobic monolith properties for passive daytime radiative cooling. *Mater. Lett.* **2023**, *352*, 135220.
(51) Li, X.; Pattelli, L.; Ding, Z.; Chen, M.; Zhao, T.; Li, Y.; Xu, H.; Pan, L.; Zhao, J. A Novel BST@TPU Membrane with Superior UV Durability for Highly Efficient Daytime Radiative Cooling. *Adv. Funct. Mater.* **2024**, *34* (23), 2315315.
(52) Shi, B.; Yin, H.; Gong, J.; Nie, Q. A novel p-n heterojunction of $Ag_2O/Bi_4Ti_3O_{12}$ nanosheet with exposed (001) facets for enhanced visible-light-driven photocatalytic activity. *Mater. Lett.* **2017**, *201*, 74−77.

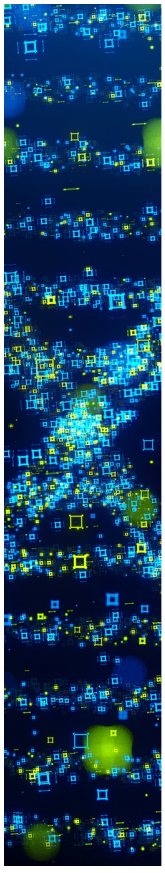

https://doi.org/10.1021/acsami.4c22615
ACS Appl. Mater. Interfaces 2025, 17, 6857−6866